Environmental Research 189 (2020) 109865

Contents lists available at ScienceDirect

Environmental Research

journal homepage: www.elsevier.com/locate/envres

Caffeine removal by *Gliricidia sepium* biochar: Influence of pyrolysis temperature and physicochemical properties

S. Keerthanan [a], Suranga M. Rajapaksha [b], Lukáš Trakal [c], Meththika Vithanage [a,*]

[a] Ecosphere Resilience Research Center, Faculty of Applied Sciences, University of Sri Jayewardenepura, Nugegoda, 10250, Sri Lanka
[b] Department of Engineering Technology, Faculty of Technology, University of Sri Jayewardenepura, Nugegoda, 10250, Sri Lanka
[c] Department of Environmental Geosciences, Faculty of Environmental Sciences, Czech University of Life Sciences Prague, Kamýcká 129, 165 00, Praha, Suchdol, Czech Republic

ARTICLE INFO

Keywords:
Water treatment
Contaminant remediation
Stimulant drug
Carbonized materials

ABSTRACT

The present study aimed to envisage the effect of physicochemical properties on the performance of *Gliricidia sepium* biochar (GBC) pyrolyzed at 300, 500, and 700 °C in the removal caffeine (CFN); a pharmaceutical and personal care product, from water. The physicochemical properties of GBC were characterized by proximate and ultimate analysis, BET, SEM, FTIR, and Raman spectroscopy. The adsorption batch experiment was carried out at various pH values (pH 3–10), mixing times (up to 24 h), and initial CFN concentration (10–500 mg/L). The FTIR analysis revealed the loss of polar functional groups on the surface of GBC derived at high temperatures. The red-shifted and blue-shifted Raman peaks indicate the condensation of small molecules on GBC. The GBC derived at 700 °C demonstrated high CFN adsorption capacity (16.26 mg/g) due to its high surface area and aromaticity. The highest adsorption of CFN was occurred at acidic pH range from 3.5 to 4.5 due to the existence of non-specific attraction between CFN and GBC. The kinetics and isotherm experimental data were fitted with Elovich and fractional power kinetic regression, Freundlich, and Temkin isotherm models, which suggested the adsorption of CFN on the GBC by mixed mechanisms; physisorption and chemisorption including π–π interactions, hydrogen bonding, n–π interactions, electrostatic attraction, and electron donor-acceptor attraction. Moreover, both surface area and aromaticity index have demonstrated a high positive correlation for CFN adsorption, signifying the importance of controlling physicochemical properties based on the end-user purpose of biochar.

1. Introduction

In order to enhance the quality of life, the pharmaceutical and personal care products (PPCPs) have received increasing demand worldwide. Pharmaceutical products including antibiotics, anti-inflammatory drugs, cytostatic drugs, blood lipid regulators, a stimulant drug, contrast media, β-blockers, and antiepileptic drugs. Also personal care products (PCPs) including antimicrobials, artificial sweeteners, ultra-violet filters, preservatives, surface activator, insect repellents, plasticizer, synthetic musks, and precursor substances of PCPs (Hyaluronic acid, butylated hydroxyanisole, β-carotene N-nitrosodimethylamine etc.) are considered as contaminants of emerging concerns in the environment (Keerthanan et al., 2020b; Liu and Wong, 2013). The annual production of PPCPs in worldwide is more than 20 million (Wang and Wang, 2016). Nowadays, PPCPs are frequently detected in the various water sources ranging from ng/L to mg/L due to excessive usage of PPCPs and their continuous release to the environment (Biel-Maeso et al., 2018; Kleywegt et al., 2019; Li et al., 2020a; Lin et al., 2016). PPCPs can create adverse effects on the health of the ecosystem, human, and non-target organisms, even at low concentrations leading them as contaminants of emerging concerns (Ebele et al., 2017).

These PPCPs are loaded into the environment through many sources, including wastewater treatment plant and sewage treatment plant, leachates from landfill, direct discharge from hospital effluents, household wastewater, animal excretion, and etc. (Dhir, 2019; Madikizela et al., 2018). The PPCPs undergo many biodegradation processes in the environment and produce several metabolites that may have different nature from the parental compounds in eco-toxicological behavior (Álvarez-Torrellas et al., 2016). Recently, the high levels of antibiotics and stimulant drugs, including sulfamethoxazole, azithromycin, and

* Corresponding author.
E-mail address: meththika@sjp.ac.lk (M. Vithanage).

https://doi.org/10.1016/j.envres.2020.109865
Received 2 April 2020; Received in revised form 14 June 2020; Accepted 17 June 2020
Available online 5 July 2020

caffeine (CFN), were found in reclaimed water at 232.1, 215.0, and 89.4 ng/L respectively in Delaware and Maryland, USA (Panthi et al., 2019). Since CFN is widely used as an active ingredient for pharmaceutical and personal care products (Herman and Herman, 2012; Lee et al., 2019), its occurrence in the aquatic environment is considerable (Kumar et al., 2019; Panthi et al., 2019) and a prodigious amount of CFN (14.2 mg/L) has already been reported in the effluent of the embalming process (Kleywegt et al., 2019).

The CFN is a naturally occurring compound that frequently presents in tea, cocoa, and coffee (Beltrame et al., 2018). However, it is widely used as a stimulant in beverages, drugs, as well as in personal care products. Due to the widespread usage of CFN, the average intake by a person is 200 mg/day. When it is ingested, the human body metabolizes CFN and excretes about 1–10% with urine (Beltrame et al., 2018). The high solubility of CFN in water (21.6 g/L) promotes the half-life of CFN from 3.5 to >100 days, depending on the environment conditions (Álvarez-Torrellas et al., 2016). Hence, CFN is widely found in the environment, which considered an emerging pollutant (Panthi et al., 2019; Papageorgiou et al., 2019). The removal of CFN from the wastewater is timely essential in a nature-friendly manner.

Biochar is a carbon-rich versatile material that can be derived from any biomass under the oxygen-limited environment at different pyrolysis temperatures (300–700 °C). It has received recent attention over activated carbon for environmental remediation of contaminants due to their specific surface area, low functional groups, and variation in physicochemical properties (Kong et al., 2019; Su et al., 2020). The high performance of biochar produced at different temperatures in the removal of environmental contaminants was reported recently by Kong et al. (2019), Li et al. (2020a, b), and Shen et al. (2020). Further, the physicochemical properties of biochar and adsorption performance mainly governed by the pyrolyzed temperature. The biochar derived at 700 °C is eager in organic pollutants remediation than those derived at 300 °C due to the higher degree of carbonization, high surface area, pore-volume, and pore-diameter at 700 °C pyrolysis temperature. (Rajapaksha et al., 2014). For instance, invasive plant biochar derived at 700 °C has a higher surface area, pore-volume, and pore diameter, and it was exhibited much higher remediation of sulfamethazine than those by the biochar derived at 300 °C (Rajapaksha et al., 2015).

The *Gliricidia sepium* biochar (GBC), a byproduct from the bioenergy plant gasified at 700–1000 °C has been applied in the removal of glyphosate from the aquatic environment (Mayakaduwa et al., 2016a). However, the variation of the physicochemical properties of GBC with pyrolysis temperature has never been reported in any previous studies. There are few studies reported the adsorptive removal of CFN by biochar produced at a single pyrolysis temperature (Anastopoulos et al., 2020; Keerthanan et al., 2020a). However, information on the effect of different pyrolysis temperature (300, 500, and 700 °C) of biochar, in the remediation of CFN from the aqueous environment, and specifically, the influence of the physicochemical properties of biochar in the removal of CFN are not existing. Furthermore, the application of GBC in the PPCPs remediation has not been reported. Therefore, using CFN as a model compound, determination of the effect of pyrolysis temperatures (300, 500, and 700 °C) on the physicochemical properties of GBC and CFN remediation is timely needed.

The biomass of *Gliricidia sepium* pyrolyzed at different temperatures was investigated for the removal of environmental contaminants. The objectives of this present study are (a) production of biochars from the *Gliricidia sepium* at different temperatures, (b) characterization of GBC and determination of physicochemical properties of GBC at various pyrolysis temperatures, (c) application of GBC as a potential CFN adsorbent in water, (d) deduction of possible CFN adsorption mechanism for GBC.

2. Materials and methodology

2.1. Chemicals

The CFN (98%) was obtained from Sisco Research Laboratories (Pvt) Ltd, India. HCl, NaOH, and spectroscopic grade KBr were purchased from Sigma Aldrich, USA. Ultra-pure water with 0.05 μS/cm conductivity was prepared by using Smart2pure 6 UV, Thermo scientific, Germany.

2.2. Biochar production

The dried biomass of *Gliricidia sepium* was ground to uniform size particles <1 mm. The ground biomass was filled and pressed to minimize the atmospheric air in a ceramic crucible with a lid. It was then closed and treated at 300, 500, and 700 °C with 7 °C/min heating rate (Rajapaksha et al., 2014; Vithanage et al., 2016) under the oxygen limited environment using a muffle furnace (P330, Nabertherm, Germany). The process was continued for 2 h once it reached the peak temperature. The obtained biochar hereafter named GBC300, GBC500, and GBC700, respectively.

2.3. Biochar characterization methods

The pH and electrical conductivity (EC) of *Gliricidia sepium* biochar (GBC) were examined in 1:5 ratios of GBC and ultrapure water suspension using digital pH (702SM Titrino, Metrohm, Swiss) and electrical conductivity meter (Orion 5 star, Thermo Scientific) respectively. The proximate analysis of biomass and GBC were carried out according to Ahmad et al. (2013). In brief, the ash content of biomass and GBC was estimated by heating at 750 °C for 1 h in an opened ceramic crucible. The mobile matter of biomass and GBC was determined by heating at 450 °C for 1 h in a lidded ceramic crucible. The moisture content of biomass and GBC was estimated by calculating the weight loss of GBC after the oven-dried to 105 °C for 24 h. The fixed matter of biomass and GBC was determined by subtracting the tally of ash, mobile, and moisture contents. The yield of GBC was estimated by calculating the ratio between dry weight of GBC and dry weight of biomass. The elemental composition, including C, H, N and S of dried biomass and ash-free dried GBC, was determined using an elemental analyzer (Vario MAX CN, elementar, Hanau, Germany) by following dry combustion method. The oxygen content of biomass and GBC was calculated by minus the total percentage of C, H, N, and S contents. These elemental analysis data were used to calculate the molar ratio of H/C, O/C, and (O + N)/C. The Brunauer-Emmett-Teller (BET) surface area, pore size, and total pore volume of GBC were analyzed using N_2 gas sorption analyzer (NOVA1200, Quantachrome Corporation, USA). Prior to N_2 gas adsorption process, the GBC was degassed for 12 h under the vacuum at 350 °C. The surface morphology of GBC was determined by Scanning Electron Microscope (SEM) images captured by Hitachi SU6600 Analytical Variable Pressure FE-SEM. The available surface functional groups of GBC before and after the CFN incorporation were determined by Fourier-transform infrared spectroscopy (FTIR; Thermo Scientific, Nicolet iS10 spectrometer, USA) from 500 to 4000 cm^{-1} of wavelength at 4 cm^{-1} resolution and 64 repetitive scans. The baseline correction, elimination of atmospheric interference, noise reduction, and peak assignment were assessed by OMNIC package (Version 6, Thermo Nicolet, USA). The surface nature of GBC before and after the CFN adsorption was investigated by a Raman spectroscope (DXR2 SmartRaman, Thermo scientific) from 500 to 2000 of Raman shift at 785 nm wavelength.

2.4. pH edge experiments

The batch experiments were conducted using 100 mL of CFN solution and 100 mg of biochar (GBC300, GBC500, and GBC700) at 25 °C. N_2 gas

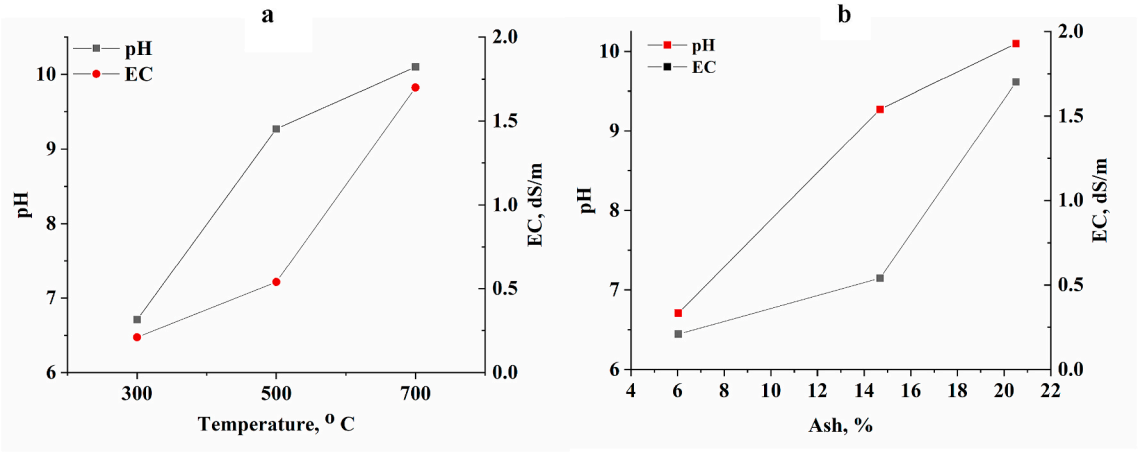

Fig. 1. The pH and electrical conductivity (EC) variation as a function of pyrolysis temperature (a) and ash content (b).

was purged to the experiment solution at a controlled flow for 30 min, in order to minimize the atmospheric CO_2 interference on the pH of the solution. The effect of pH in the CFN adsorption by biochar was investigated at various initial pH ranges (pH 3–10). The initial pH of solutions was adjusted with 0.1 M HCl, and 0.1 M NaOH solutions. The mixture of 50 mg/L of CFN solution and 1 g/L dosage of GBC300, GBC500, and GBC700 separately were kept in the shaker at 150 rpm for 12 h to reach the equilibrium. Afterward, the equilibrium pH of mixtures was measured in order to obtain the optimum pH. All the mixtures were centrifuged at 2500 rpm and filtered using a 0.45 μm syringe filter (Labfil-PTFE hydrophobic, C0000300, China). The equilibrium concentration of CFN in each solution was determined by using Thermo Scientific GENESYS 10S UV Visible spectrophotometer at 272 nm. Each run was carried out in triplicates, and its average values were calculated.

2.5. Adsorption kinetic experiments

The kinetic of CFN adsorption for each GBC300, GBC500, and GBC700 were carried out with 1 g/L dosage of biochar and 50 mg/L CFN solution at 25 °C with the optimum pH 4.5. The mixing times were varied during the experiments for 5, 10, 20, 30, 45 min, and also for 1, 1.5, 3, 6, 8, 10, 12, and 24 h. At the end, in each mixture, the equilibrium concentration of CFN was determined using UV Visible spectrophotometer at 272 nm.

2.6. Adsorption isotherm experiments

In the CFN adsorption isotherm experiment, CFN solutions with various concentrations ranging from 10 to 500 mg/L were shaken with 1g/L dosage of each GBC300, GBC500, and GBC700 separately for 12 h at 25 °C under the optimum pH 4.5.

2.7. Calculation and data modeling

The kinetic experiment results were modeled with a nonlinear equation of Elovich and fractional power regression. The adsorption isotherm data were fitted with Temkin and Freundlich nonlinear regressions in order to understand the CFN adsorptive mechanism by GBC types. All adsorption experiment data were modeled by using the Origin statistical software package (version 8.0).

The adsorption capacity of CFN at the equilibrium (q_e, mg/g), at specific times (q_t, mg/g), and adsorption efficiency of CFN (A%) of each GBC were calculated using equations (1), (2), and (3), respectively (Li et al., 2018).

$$q_e = (C_i - C_e) \times (V / M) \quad 01$$

Table 1
The physio-chemical properties of biomass and each GBCs.

Characteristics	Biomass	GBC300	GBC500	GBC700
(a) Proximate analysis				
- pH	6.05 ± 0.22	6.71 ± 0.17	9.27 ± 0.04	10.1 ± 0.12
- EC (dS/m)	0.94 ± 0.1	0.21 ± 0.02	0.54 ± 0.04	1.7 ± 0.08
- Ash %	2.37 ± 0.17	6.03 ± 0.08	14.68 ± 0.1	20.51 ± 1.96
- Mobile matter %	76.46 ± 4.95	28.58 ± 0.8	21.79 ± 0.09	23.81 ± 0.24
- Fixed matter %	11.47 ± 0.94	61.8 ± 0.29	60.85 ± 0.39	54.4 ± 1.92
- Moisture %	9.68 ± 0.31	3.57 ± 0.25	2.66 ± 0.04	1.27 ± 0.05
- Yield %	–	39.58 ± 1.04	26.24 ± 0.55	22.79 ± 0.71
(b) Ultimate analysis				
- C %	52.10	75.46	73.29	92.75
- H %	7.03	4.76	3.55	1.46
- O %	40.08	19.02	22.28	4.92
- N %	0.72	0.72	0.84	0.73
- S %	0.05	0.04	0.04	0.14
- Molar H/C	0.135	0.063	0.048	0.016
- Molar O/C	0.769	0.252	0.304	0.053
- Molar (O + N)/C	0.783	0.261	0.315	0.055
(c) BET analysis				
- Surface area (m^2/g)	–	1.02	76.30	216.40
- Pore volume (cm^3/g)	–	0. 0012	0.0052	0.1097
- Pore size (Å)	–	383.6	703.1	766.5

$$q_t = (C_i - C_t) \times (V / M) \quad 02$$

$$A\% = (C_i - C_e) \times (100 / C_i) \quad 03$$

where, C_i, C_e, and C_t are the concentration of CFN initial, at the equilibrium, and at specific time (t) in mg/L. V is the volume of CFN solution in liters, and M is the mass of GBC in grams.

3. Results and discussion

3.1. Biochar characterization

3.1.1. Effect of pyrolysis temperature on the physicochemical properties of GBC types

The pH and EC of GBC types were gradually elevated with the pyrolysis temperatures from 300 to 700 °C (Fig. 1a and Table 1a) due to alkali salts separation from the organic material and elimination of acidic functional groups at high temperatures (Rajapaksha et al., 2015).

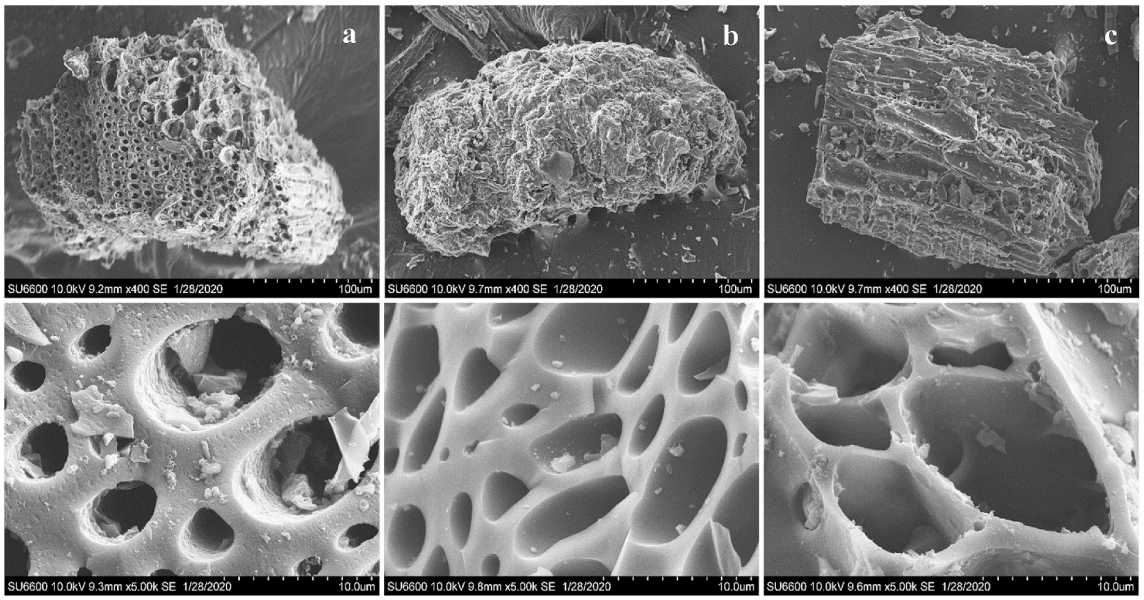

Fig. 2. The SEM images of GBC300 (a), GBC500 (b), and GBC700 (c) at different magnification; x400 (top line) and x5000 (bottom line).

Generally, increase of pyrolysis temperature caused an increase in ash content of biochar (Mayakaduwa et al., 2016b; Tomczyk et al., 2020). The ash content of GBC also increased from 6.03 to 20.51% with an increase of pyrolysis temperature (Table 1a). This may be due to increase the concentration of inorganic substances and combustion residues of organic matter. Mainly, mineral matters derived from Na, K, Ca, Mg, P, S, Zn, Fe, Mn, etc. (Ahmad et al., 2014) were remained in the GBC ash following pyrolysis due to increase of volatilization. Moreover, the yield % of GBC decreased with pyrolysis temperature increases, this elaborated that the fact of escaping of volatile material from the feedstock and high degree of solid degradation during the pyrolysis (de Souza dos Santos et al., 2020). The proximate and ultimate analysis of GBC pyrolyzed at various temperatures are displayed in Table 1.

The carbon content of GBC700 was relatively higher than those values of GBC300 and GBC500 (Table 1b). The H and O contents of GBC types were decreased with the elevated pyrolysis temperature suggesting elimination of H_2, CO_2, CO, H_2O, and CH_4 from the feedstock (Ahmad et al., 2012; Zhang et al., 2020), but no significant changes were observed on the N content of GBC types during the pyrolysis (Table 1b).

As reported before, both the aromaticity and polarity indices of GBC types is determined by the molar ratio of H/C and O/C and (O + N)/C, respectively (Zhang et al., 2020). Therefore, the H/C ratio was decreased gradually with pyrolysis temperature indicating the possible condensation of aromatic rings on the surface of GBC during the pyrolysis (Zhao et al., 2018) (Table 1b). The formation of aromatic rings on GBC surface was confirmed by the FTIR (formation of out of plane C–H bending vibration peak for aromatic ring at 864 cm^{-1}, increase in the intensity of C–H bending vibration peak at 1443 cm^{-1}, and shifting of C═C stretching peak for aromatic ring to 1567 cm^{-1}, confirmed the formation of aromatic nature on GBC surface) and Raman spectroscopy analysis (the blue shift of G band and red shift of D band indicates the condensation of small molecules into an aromatic cluster and oxygenated functional groups defect on the amorphous surface of GBC). The O/C and (O + N)/C ratios were also decreased compared to the results from low pyrolysis temperatures (Table 1b). The polarity of biochar diminished due to the loss of polar functional groups during the pyrolysis, whereas the stability of GBC showed an increase with decreasing O/C ratio (Zhao et al., 2018). The BET surface area of GBC was increased

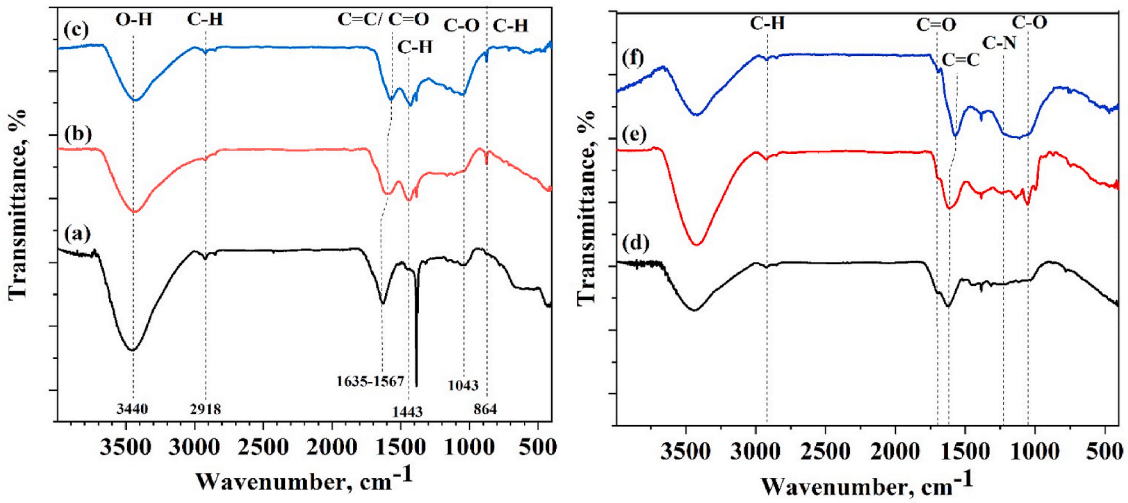

Fig. 3. The FTIR spectra of pristine GBC types; (a) GBC300, (b) GBC500, and (c) GBC700 and CFN-GBC types; (d) CFN-GBC300, (e) CFN-GBC500, and (f) CFN-GBC700.

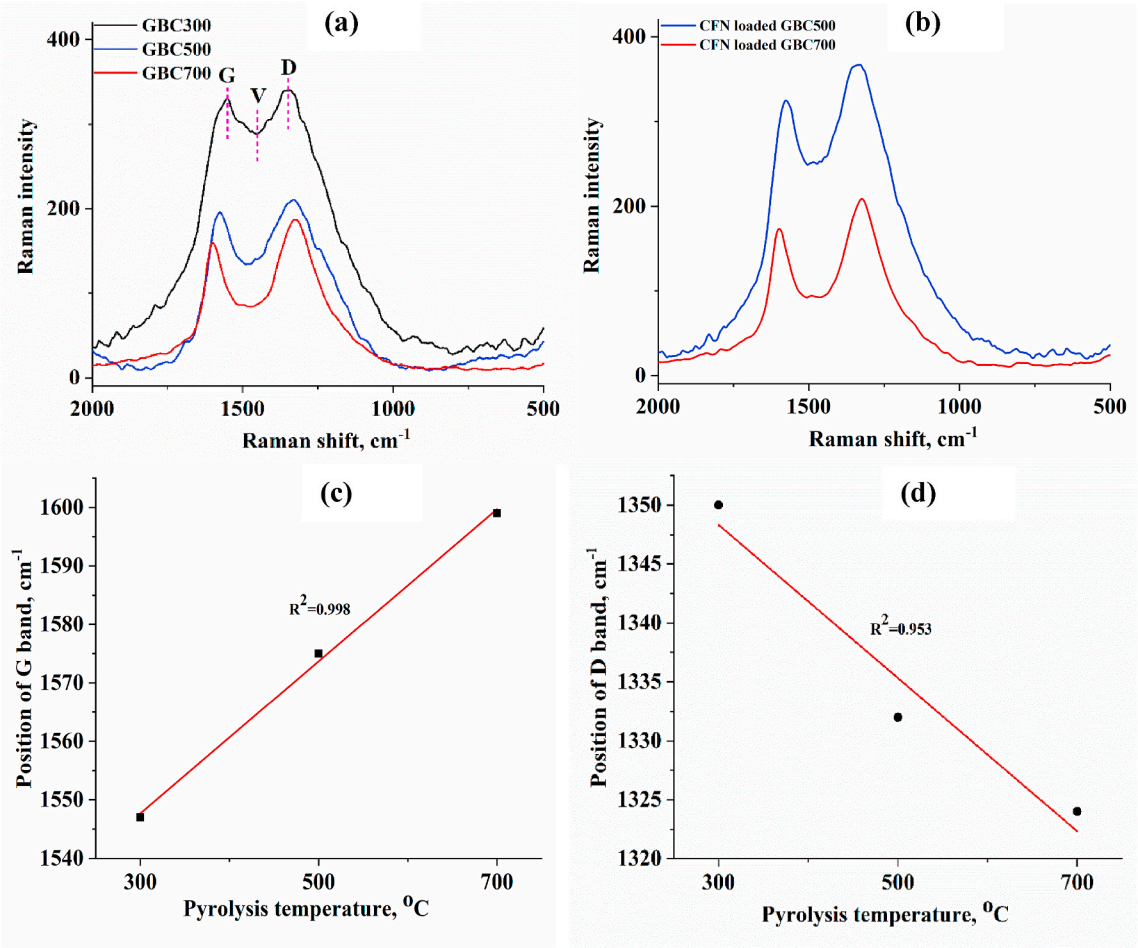

Fig. 4. The Raman spectra of pristine GBC (a) and CFN loaded GBC (b) and linear relationship between the position of G (c) and D (d) bands with pyrolysis temperature. Note: Raman spectrum of CFN loaded GBC300 is not reported above due to the fluorescence effect during the analysis.

from 1.02 to 216.4 m^2/g when pyrolysis temperature increased from 300 to 700 °C (Table 1c). It may be due to the formation of voids structures on the GBC surfaces which was observed during SEM. The pore volume of GBC increased with rising pyrolysis temperature (Table 1c) which strongly related to increase the surface area of GBC, as stated Ahmad et al. (2013). The pore size also increased significantly with pyrolysis temperature. As defined in Ahmad et al. (2013), the pore size <20 Å suggested as micro-pores, whereas pore size 20–500 Å suggested as meso-pores. The pore size >500 Å defined as macro-pores. The pore size of GBC300, GBC500, and GBC700 were 383.6, 703.1, and 766.5 respectively, indicates GBC300 was dominated by meso-pores whereas, GBC500 and GBC700 were dominated by macro-pores.

3.1.2. Surface morphology of GBC

The SEM images of GBC snapped at different magnifications (x400 and x5000) are represented in Fig. 2. Notable changes were observed on the surface of GBC produced at different pyrolysis temperatures due to the formation of voids. The porosity of GBC in the heterogeneous surface was increased as the pyrolysis temperature increases from 300 to 700 °C. Moreover, the formation of macro-sized holes can be clearly seen in the GBC700. This may be due to the escaping of mobile matter from the feedstock during the pyrolysis (Ahmad et al., 2012), since the raw feedstock contains 76.46% of mobile matter (Table 1a). This positive direction in changes of surface porous morphology on GBC surface with pyrolysis temperature could be the fact to increase the BET surface area of GBC.

3.1.3. Surface functional groups of GBCs

The pyrolysis temperature strongly influenced the functional group density of the GBC surface (Fig. 3). In all GBC types, two distinct bands at 3440 cm^{-1} and 2918 cm^{-1} were observed (Fig. 3a–c). The characteristic stretching peak at 3440 cm^{-1} could be indicated the presence of hydroxide groups belonging to phenolic and/or carboxylic group (Álvarez et al., 2015) and its shape was narrowed by increasing the pyrolysis temperature from 300 to 500 °C. The relative intensity of the band at 2918 cm^{-1} of the aliphatic –C–H stretching was decreased with the pyrolysis temperature. These changes on peaks at 3440 cm^{-1} and 2918 cm^{-1} demonstrated the dehydration of lignin and/or cellulose compounds, as well as structural changes on the aliphatic compounds during the pyrolysis (Zhao et al., 2018). The stretching peak at 1635 cm^{-1} which described the presence C═O group of carboxylic acid, conjugated ketone, and/or quinone (Zhang et al., 2020) on the GBC300 surface (Fig. 3a). This peak shifted to 1567 cm^{-1} (belong to aromatic C═C stretching band) when the pyrolysis temperature increased to 700 °C (Fig. 3c). This peak shifting support the availability of aromatic groups on the GBC700 surface at higher pyrolysis temperature. Concurrently, the formation of new aromatic –C–H bending peak at 1443 cm^{-1} on the surface of both GBC500 (Fig. 3a) and GBC700 (Fig. 3c) also indicate the aromatic surface of the GBC (Pavia et al., 2001). It was further confirmed by the formation of a new out of plan –C–H bending peak at 864 cm^{-1} of the aromatic ring (Fig. 3a–c). The stretching vibration peak at 1043 cm^{-1} belong to C–O ascribed the presence of phenolic and/or carboxylic groups on the GBC surface (Zhang et al., 2014). Based on the literature, the degree of condensation of compounds much higher with increasing pyrolysis temperature (Zhao et al., 2018).

Table 2
The intensity ratios of $\frac{I_D}{I_G}$, $\frac{I_V}{I_G}$, and $\frac{I_V}{I_D}$ of GBC300, GBC500, and GBC700.

Ratios	Pristine GBCs			CFN incorporated GBCs		
	GBC300	GBC500	GBC700	GBC300	GBC500	GBC700
ID/IG	1.039	1.077	1.207	–	1.143	1.224
IV/IG	0.858	0.675	0.488	–	0.749	0.490
IV/ID	0.826	0.626	0.404	–	0.656	0.400

The CFN adsorbed GBC were also characterized by FTIR. As in Fig. 3d–f, the new peaks were appeared for CFN. The stretching peaks of C═O and C–N peaks at 1696 and 1224 cm^{-1}, respectively supported the CFN adsorption on the surface of GBC (Keerthanan et al., 2020a). Furthermore, the increasing and broadening of peak intensities of stretching of –C–H, C═C, and C–O at 2920, 1657, and 1053 cm^{-1}, respectively, also confirmed the incorporation of CFN with GBC.

3.1.4. Raman analysis of GBC

The Raman spectroscopy has been used to investigate the changes in the electronic structure and carbon material defects in the biochar during the pyrolysis (Jiang et al., 2013). The first order range (500-2000 cm^{-1}) Raman spectra of pristine GBC and CFN adsorbed GBC are provided in Fig. 4a and b. Generally, monocrystalline carbonaceous material would show only one peak at around 1580 cm^{-1}, while disordered amorphous carbonaceous material shows two peaks at 1350 and 1600 cm^{-1} (Ncibi et al., 2014). In this study, the Raman spectra of GBC show two peaks at 1600–1550 cm^{-1} (G band) and 1350–1325 cm^{-1} (D band) (Guizani et al., 2017a). It confirmed the disordered amorphous carbon formed in GBC during the pyrolysis process. Furthermore, both G and D bands' intensities become weaker with rising pyrolysis temperature due to the growth of aromatic compounds on the surface of GBC (Yip et al., 2011).

The wave number of G band was increased (blue shift) along with the pyrolysis temperature, and this accounted for the volatile molecules that underwent the condensation process and precipitated on the surface of GBC (Liu et al., 2014). As shown in Fig. 4c, the blue shifted G band has a linear correlation ($r^2 = 0.998$) with pyrolysis temperature. On the other hand, the D band was red shifted along with the pyrolysis temperature (Fig. 4d) due to defects of oxygenated structure on the GBC (Guizani et al., 2017b). The red shifted D band also has a linear correlation with pyrolysis temperature, as shown in Fig. 4d. A similar band shifting pattern was also previously reported with harakeke char produced at 430, 550, 700, 900, and 1000 °C (McDonald-Wharry et al., 2013).

According to literatures, the investigation of D and G bands has done by calculating the intensity ratio of $\frac{I_D}{I_G}$, $\frac{I_V}{I_G}$, and $\frac{I_V}{I_D}$ where I_D, I_G, and I_V are the intensities of D, G, and V bands (Guizani et al., 2019; Kawakami et al., 2005). The calculated ratios in this study are listed in Table 2. The value of $\frac{I_D}{I_G}$ has gradually been increased with the pyrolysis temperature. The value also directly proportional to number of ordered compounds, which indicates the ordered graphene structures in GBC (Mendonça et al., 2017), and their formation were increased with pyrolysis temperature (Yang et al., 2018). On the other hand, the values of $\frac{I_V}{I_D}$ dwindled sharply when pyrolysis temperature was increased from 300 to 700 °C. Based on these observations it is postulated that the condensation of small aromatic ring molecules <6 rings into aromatic clusters during the pyrolysis (Guizani et al., 2019). Similar to $\frac{I_V}{I_D}$ values, the values of $\frac{I_V}{I_G}$ were reduced gradually (Table 2) with the pyrolysis temperature. It also suggests the formation of aromatic compounds in GBC during the pyrolysis (McDonald-Wharry et al., 2013). The Raman data concluded that the pyrolysis temperature has affected the properties of GBC, and their amorphous carbonaceous materials (Maliutina et al., 2018).

3.2. Effect of pyrolysis temperature on CFN adsorption

As shown in Fig. 5a, the CFN adsorption capacities of both GBC300 and GBC500 are almost similar (≈4 mg/g). However, it was abruptly approached 4-fold increase from 4 to 16.26 mg/g when high-temperature pyrolysis at 700 °C. The CFN adsorption efficiency of GBC also followed the similar pattern as the adsorption capacity. These results suggest the influence of pyrolysis temperature on boosting CFN adsorption by GBC from the water. Lower surface area, and higher molar ratio of H/C and O/C of GBC300 and GBC500 when compare with GBC700 could be the key reasons for the both GBC300 and GBC500 exhibited lower and similar CFN adsorption capacity. The higher CFN adsorption by GBC700 may be due to the changes in the morphology of the GBC surface such as widening and formation of internal porous structure (Fig. 2) to have higher surface area (Table 1). Further variations such as functional groups (Fig. 3) and electronic structure changes (Fig. 4a) on the GBC surface along with the pyrolysis temperature may also have affected the CFN adsorption.

3.3. Determination of optimum pH for CFN adsorption

As demonstrated in Fig. 5b, the maximum adsorption capacity was observed between pH 4 and 5. However, it was significantly decreased by increasing pH from 7 to 10 showing high pH dependency of CFN adsorption. According to Beltrame et al. (2018), the predominant species of CFN until pH 5.5 is neutral (CFN^0), whereas negative form

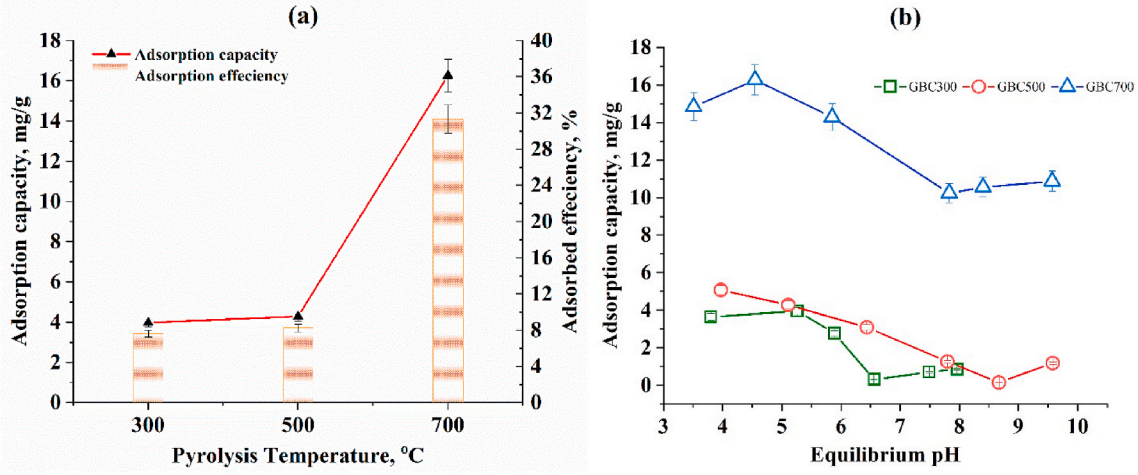

Fig. 5. The pattern of CFN adsorption capacity and CFN adsorption efficiency of GBC as the function of pyrolysis temperature (a) and the effect of pH on the CFN adsorption capacity at 25 °C (b). (The error bars represent the calculated ± standard error of mean (n = 3)).

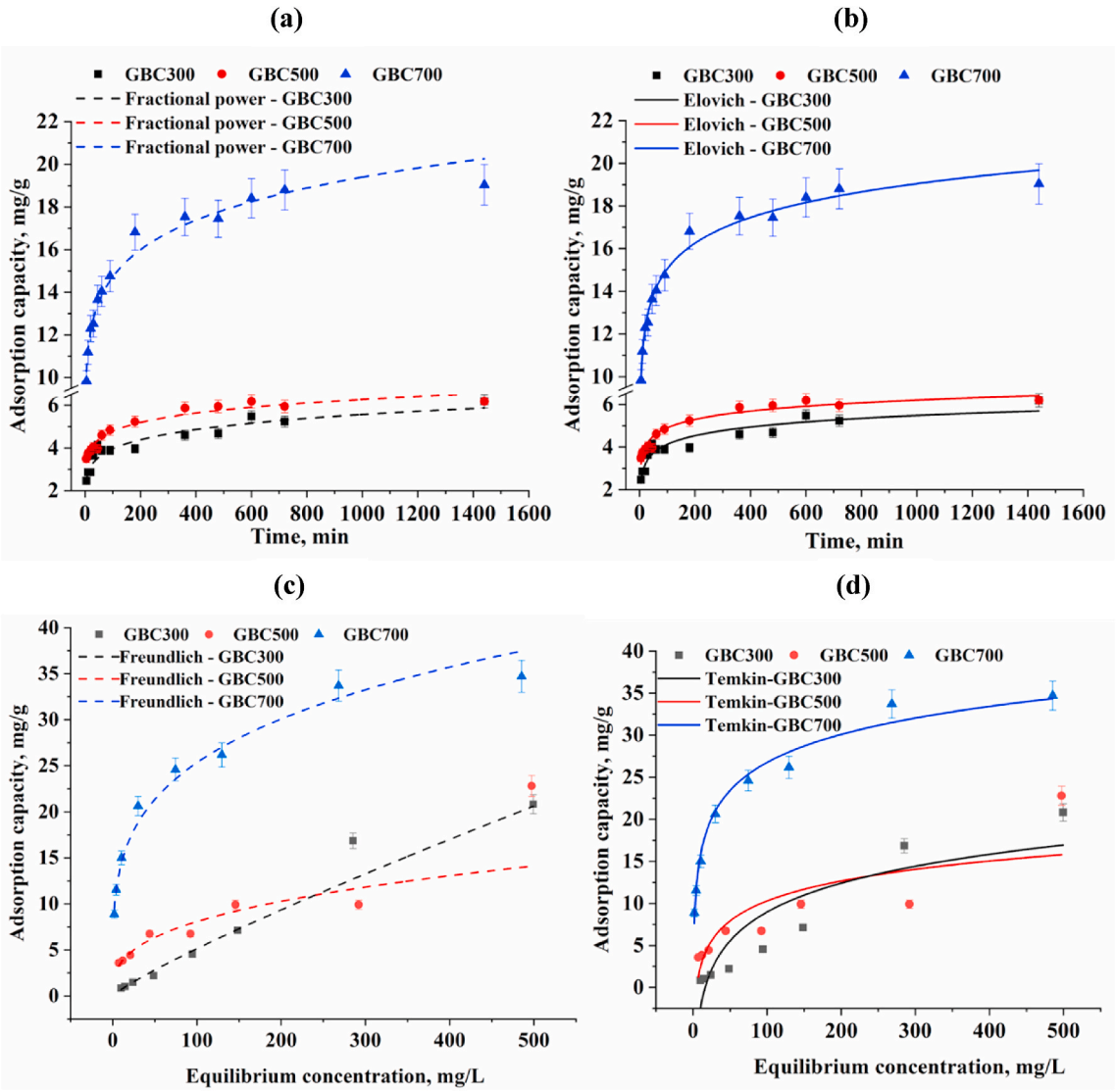

Fig. 6. The fitted kinetic models (a and b) and the isotherm fitted models (c and d) with 1 g/L dosage of GBC at pH 4.5 and 25 °C. (The error bars represent the calculated ± standard error of mean (n = 3)).

(CFN^-) predominantly exists above pH 5.5. At pH 4.5, the neutral species of CFN interacted with positively charged GBC surface via the non-specific attractions, such as hydrogen bonding, π-π interaction (Álvarez-Torrellas et al., 2016), and n-π interaction (Tran et al., 2017a). At pH above 5.5, the negatively charged CFN species in the solution and negatively charged GBC repelled each other resulting the less favorable non-electrostatic interactions. Thus, the pH 4.5 was selected to conduct the series of adsorption studies under the same operational conditions.

3.4. Effect of mixing time on CFN adsorption

As represented in Fig. 6a and b, the CFN adsorption capacity was increased with increasing mixing time. The removal of CFN by GBCs was rapidly increased until 180 min and then it was reached an equilibrium. This may be due to the availability of large amount of active sites on GBC at the beginning of mixing and it reached an equilibrium due to the limited number of active sites on the GBC with time (Ashiq et al., 2019).

The experiment data was modeled with Elovich and fractional-power to understand the adsorption behavior between CFN and GBC. Both Elovich and fractional-power models were well fitted with experimental data based on the regression coefficient (r^2) > 95% and lower chi^2 (Table 3). The Elovich model described the adsorption of CFN took place at the heterogeneous surface of GBC via the chemisorption (Netzahuatl-Muñoz et al., 2015). The obtained r^2 and chi^2 values for the Elovich model are 0.99, 0.95, and 0.91of GBC700, GBC500, and GBC300 respectively. The initial adsorption rate of CFN (α) was increased in the order of GBC300, GBC500, and GBC700 (Table 3). The desorption constant related to extending of active sites on the adsorbent decreased in the order of GBC300, GBC500, and GBC700, suggesting the involvement of surface functional groups in the removal of CFN (Inyinbor et al., 2016). The fractional-power kinetic model also fitted with experiment data, and it describes the adsorption of CFN that occurs on homogeneously surface of GBC (Mayakaduwa et al., 2016a). Constant *v* obtained as less than unity in fractional-power kinetic, suggesting the favorability of CFN adsorption (Inyinbor et al., 2016). Hence, the kinetic models suggested the adsorption of CFN onto the GBC surface via the chemisorption, involving electron transfer mechanism between surface functional groups and CFN molecule (Beltrame et al., 2018).

3.5. Effect of the initial concentration of CFN on CFN adsorption

Fig. 6c and d presents CFN adsorption isotherm results of GBC300, GBC500, and GBC700. The GBC300 and GBC500 showed an almost similar in the CFN adsorption capacity, whereas the GBC700 recorded

Table 3
The kinetic and isotherm regressions for adsorption of CFN by GBCs at 25 °C and pH 4.5

Models	Non-linear equations	Description	Parameter	Parameter values		
				GBC300	GBC500	GBC700
Adsorption kinetics						
Elovich (Tran et al., 2017c)	$q_t = \frac{1}{\beta}\ln(1+\alpha\beta t)$	α: initial CFN adsorption rate (mg/g × min).	α	6.64 ± 3.96	33.32 ± 17.59	102.3 ± 28.46
		β: desorption constant related to extent of surface coverage (g/mg).	β	1.70 ± 0.16	1.77 ± 0.12	0.58 ± 0.02
			r^2	0.91	0.95	0.99
			Chi^2	0.11	0.05	0.14
Fractional power (Netzahuatl-Muñoz et al., 2015)	$q_t = Kt^v$ $k = K^*v$	*K*: constant (mg/g)	*K*	2.00 ± 0.12	2.79 ± 0.10	8.45 ± 0.22
		v: rate constant (1/min)	*v*	0.15 ± 0.01	0.12 ± 0.01	0.12 ± 0.01
		k: specific rate constant (mg/g × min)	*k*	0.30	0.33	1.01
			r^2	0.93	0.96	0.98
			Chi^2	2.29	0.85	0.44
Adsorption isotherms						
Temkin (A.O, 2012)	$q_e = \frac{RT}{b}\ln(A_T C_e)$ $B = \frac{RT}{b}$	*b*: Temkin constant	*b*	500 ± 98	723 ± 199	515 ± 28
		A_T: Temkin equilibrium binding constant (L/mg)	A_T	0.06 ± 0.02	0.20 ± 0.16	2.62 ± 0.70
		R: gas constant (J/mol × K)	B	4.96	3.43	4.81
		T: temperature (K)	r^2	0.82	0.69	0.98
		B: adsorption energy (J/mol)	Chi^2	12.92	14.35	1.90
Freundlich (Bordoloi et al., 2017)	$q_e = k_f C_e^n$	k_f: Freundlich constant related to the adsorption capacity (mg/g)/(mg/L)^n	k_f	0.10 ± 0.02	1.64 ± 0.37	8.11 ± 0.38
			n	0.86 ± 0.05	0.35 ± 0.05	0.25 ± 0.01
		n: adsorption intensity	r^2	0.95	0.84	0.98
			Chi^2	10.58	15.61	1.59

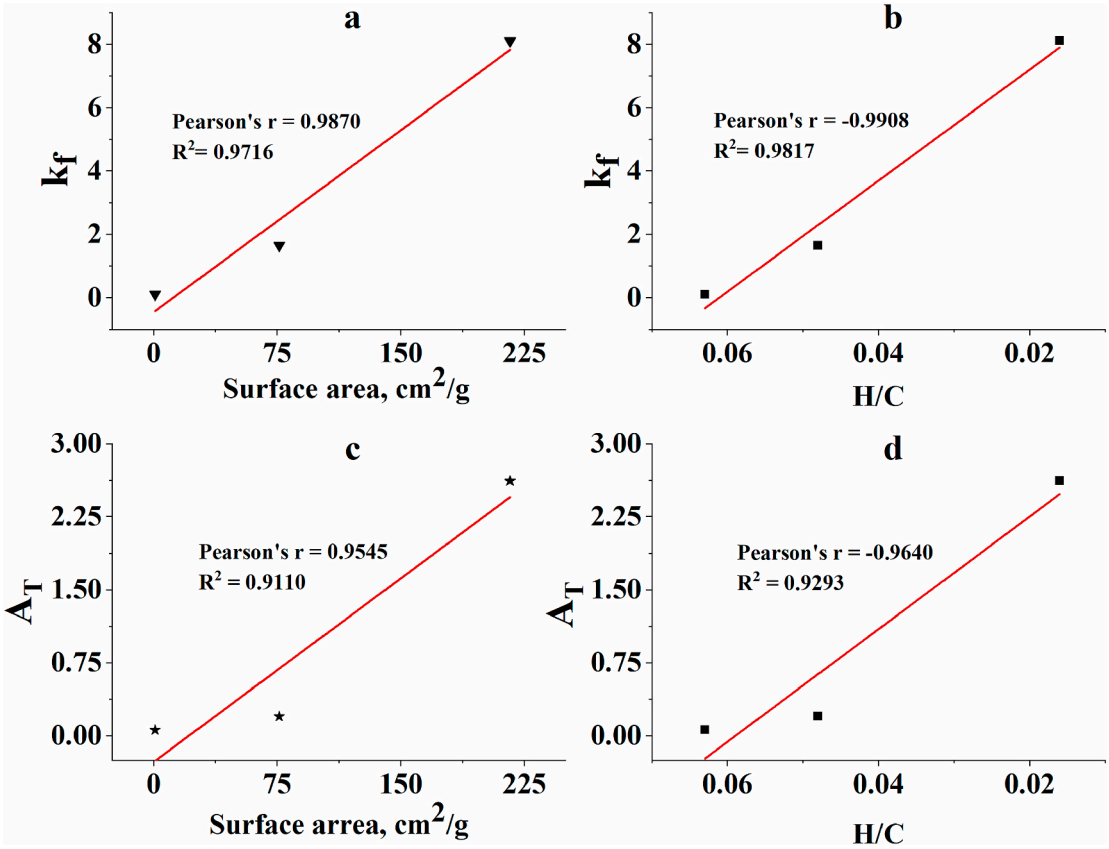

Fig. 7. The linear correlation of estimated Freundlich constant (k_f) and Temkin equilibrium binding constant (A_T) as a function H/C and surface area of GBCs.

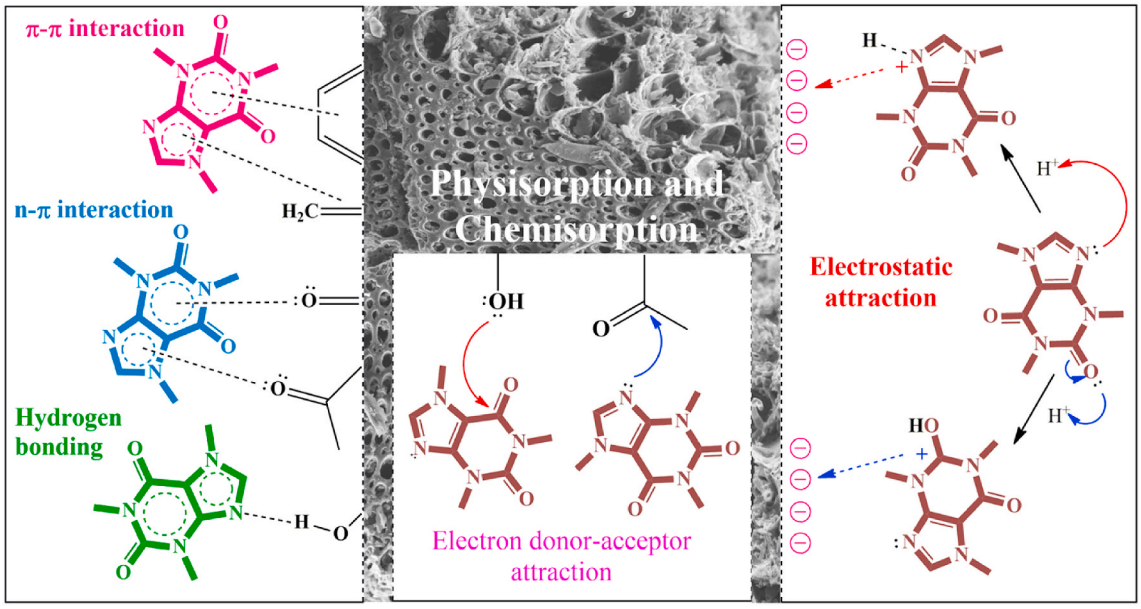

Fig. 8. The graphical presentation of possible mechanism employed in the removal of CFN by GBC.

the highest CFN adsorption capacity as expected based on the physico-chemical properties of GBC. When the initial concentration of CFN was increased, the number of CFN molecules was increased than the number of surface-active sites on GBC surface resulting the low CFN adsorption.

The isotherm results were investigated through the non-linear regression of Freundlich and Temkin and these parameters are given in Table 3. Among the tested GBC types, the GBC700 displayed the highest CFN adsorption efficiency based on the high regression coefficient (r^2) > 95% and lowest chi^2 (Table 3) (Mayakaduwa et al., 2016b). The Freundlich isotherm described the adsorption of CFN occurred via physical interaction at the heterogeneous surface of GBC. The k_f value of GBC700 was relatively higher than those value of GBC300 and GBC500, and this indicate the high affinity of CFN to the GBC700. Similarly, the adsorption intensity (n) value obtained from Freundlich model was <1, which indicates the interaction of CFN with the surface of GBC is favorable (Ahmad et al., 2013). Moreover, the n value was decreased by increasing the pyrolysis temperature. A similar trend was reported by a previous study while investigating the removal of sulfamethazine by invasive plant-derived biochar (Rajapaksha et al., 2015).

The non-linear regression of the Temkin isotherm model was fitted with experimental results along with the Freundlich model based on the regression coefficient and chi^2. The Temkin model describes the CFN adsorption by GBCs is due to the generation of chemical forces between CFN and GBC (Biswas et al., 2007). This model previously presumed the linear decrease of adsorption heat with surface coverage is due to the interaction between adsorbent and adsorbate (Rajapaksha et al., 2015). Both Freundlich and Temkin isotherm models suggested that the efficient removal of CFN has been designated to the GBC700, which was driven through the mixed mechanism of both physisorption and chemisorption.

3.6. CFN adsorption and GBC properties

The linear relationship of Freundlich constant (k_f) related to CFN adsorption capacity and Temkin binding constant (A_T) as the function of GBC properties are indicated in Fig. 7. A strong positive linear correlation was observed between surface area, k_f, and A_T (Pearson's r > 0.95), which indicated that the surface area of GBC affects the adsorption of CFN. However, the aromaticity index (H/C) showed a negative linear correlation with k_f, and A_T (Pearson's r < −0.95) indicating the high degree of carbonization, which took place on GBC at high temperature. These observations may be due to the lack of oxygen contained functional groups on the GBC, which derived at high pyrolysis temperature. Biochar pyrolyzed at low temperature has rich in oxygen contained functional groups, which holds water molecules via hydrogen bonds causing the lower CFN adsorption, whereas the biochar derived at high temperature indicated high CFN adsorption due to its hydrophobic nature (Rajapaksha et al., 2015).

3.7. The mechanism of CFN adsorption

In this study, the predicted kinetic and isotherm data suggested that the functioning of both physical and chemical forces in the removal of CFN by GBC derived from various pyrolysis temperatures. The physical interaction might be due to the π–π interactions, hydrogen bonding, n–π interactions, weak van der Waals forces, and dipole-dipole interactions between the CFN molecules and GBCs (Essandoh et al., 2015; Tran et al., 2017c). The adsorption mechanism was proposed with the support of FTIR results obtained for the pristine GBC and CFN treated GBC, shown in Fig. 3. The π–π electron–donor-acceptor interaction also known as π–π interaction can exist between the π electron-rich surface of GBC and the π electron cloud of CFN heterocyclic ring (Tran et al., 2017a), evidenced by the broadening and increasing intensity of aromatic C═C stretching vibrations at between 1560 and 1610 cm^{-1} in CFN treated GBC. Since the CFN molecule has two fused aromatic rings, it might be contributed to the π electron delocalization system in the GBC surface, since it showed an increase in peak intensities. The presence of π–π interaction between CFN and biochar was reported in a previous study of Correa-Navarro et al. (2019). As discussed in Tran et al. (2017b), the n–π electron-donor-acceptor interaction is also known as n–π interaction, which occurs between long pair electron-rich atoms such as oxygen on the surface of GBC and π electron cloud of CFN molecules.

Hydrogen bonding is another adsorptive mechanism employed in the removal of CFN by GBC. Generally, the hydrogen bonding occurs between an H-donor group (hydroxide group on the GBC) and H-acceptor (oxygen/nitrogen in the CFN molecule) (Jiang et al., 2018) as elaborated in Fig. 8. The notable change observed in the FTIR analysis might confirm the existence of H-bonding during the CFN adsorption process. The shifting of –OH stretching vibration from 3440 to 3422 cm^{-1} in CFN treated GBC (Fig. 3) indicates the presence of H-bonding in the CFN adsorbed GBC since strong H-bonding decreases the stretching vibrations (Yadav, 2002).

Table 4
Comparison of CFN adsorption capacity by various adsorbents.

Water types	Adsorbent (dosage)	Pyrolysis temp, °C	Experiment conditions	Initial concentration of CFN, mg/L	Maximum adsorption capacity, mg/g	References
Synthetic water	Pine needle biochar (1.67 g/L)	650	pH: 4 T: 298 K AT: 48 h	50	5.35	Anastopoulos et al. (2020)
Synthetic water	Mesoporous activated carbon fiber (1 g/L)	300 and 500	pH 5.80 T: 298 K AT: 240 min	25–500	155.5	Beltrame et al. (2018)
Synthetic water	MgAl-LDH/biochar composite (4 g/L)	–	pH 12 T: 313 K AT: 2 h	5–200	21.4	dos Santos Lins et al. (2019)
Synthetic water	Carbon xerogel modified with copper acetate (0.4 g/L)	–	T: 298 K	6.5–150	107	Ptaszkowska-Koniarz et al. (2018)
Real water (industrial wastewater)	Pine needle biochar (1.67 g/L)	650	pH: 7.8 T: 298 K AT: 24 h	50	1.41	Anastopoulos et al. (2020)
Synthetic water	Steam activated tea waste biochar (1 g/L)	700	pH: 3.5 T: 298 K AT: 12 h	50	15.4	Keerthanan et al. (2020a)
Synthetic water	Fique bagasse biochar (10 g/L)	850	T: 293 K AT: 24 h	50	5.1	Correa-Navarro et al. (2020)
Reclaimed water	Pinyon Pine Juniper wood biochar (40 g)	No controlled temperature	**Parameters of reclaimed water (Fixed bed column experiment)** pH: 7.9 T: 294.5 K [CFN]: 135.2 ng/L		0.4	Yanala and Pagilla (2020)
Synthetic water	Water hyacinth biochar (2 g/L)	350	T: 298 K	5	2	Emily Chelangat Ngeno et al. (2016)
Synthetic water	GBC (1 g/L)	700	pH: 4.5 T: 298 K AT: 12 h	50	16.3	**This study**

T: Temperature, AT: Agitated time.

Another possible adsorptive mechanism took place via the electron donor-acceptor between GBC and CFN molecule. The N atom which not attached with methyl group in the five membered ring of CFN can be acted as electron donor to the C═O group attached to GBC surface, whereas the C═O group in six membered ring of CFN can be functioned as electro acceptor. These interactions have confirmed through the FTIR analysis (Fig. 3). The new appearance of C–N stretching vibration at 1224 cm^{-1} in the CFN treated GBC demonstrated that the CFN donated electrons to the GBC surface, while the intensity arising of C–O frequency and peak shifting from 1043 to 1053 cm^{-1} in the CFN treated GBC showed that the CFN acted as an electron acceptor from the GBC as represented in Fig. 8. Also, electrostatic attraction employed between negatively charged GBC and CFN molecule at pH 4.5. The existence of electrostatic attraction between biochar and CFN molecule previously proposed by Anastopoulos et al. (2020) and Keerthanan et al. (2020a).

4. Comparison of CFN adsorption capacity by various biochar from synthetic and real wastewater

As listed in Table 4, There are number of studies have been investigated the adsorptive remediation of CFN from the aquatic media using different types of biochar produced at various conditions. Most of investigation was carried out the remediation of CFN in a single-contaminant system (Correa-Navarro et al., 2020; Keerthanan et al., 2020a). Few studies were reported the remediation of CFN from wastewater effluent (Anastopoulos et al., 2020; Yanala and Pagilla, 2020). The present study exhibited higher adsorption capacity from a single-contaminant system prepared at laboratory than other biochar presented in Table 4. In case of real wastewater/multi-contaminant system, the removal capacity became less in the presence of other contaminants compare to the single-contaminant system. For instance, Anastopoulos et al. (2020) reported, the CFN adsorption capacity by pine needle biochar was 4-time decreased in industrial wastewater. Another study of Yanala and Pagilla (2020) reported, the continues flow of reclaimed water containing 135.2 ng/L of CFN through a fix bed column prepared using pinyon pine juniper wood biochar, removed 0.396 mg/g of CFN. Thus, the GBC as a novel adsorbent could be provided an effective way to remove the CFN from the wastewater in the presence of multi contaminants.

5. Conclusions and recommendations

In this study, *Gliricidia sepium* woody biochar was successfully produced at various pyrolysis temperatures. The GBC700 shows higher aromatic nature than both GBC500 and GBC300 and it was confirmed by FTIR and Raman spectroscopy analysis. Among studied GBC types, GBC700 showed the highest CFN adsorption capacity due to the improvement of physicochemical properties. The adsorption of CFN is governed by the pH of the medium, and the highest adsorption 16.3 mg/g was recorded in the acidic pH 4.5. Adsorption kinetic model fits the Elovich and fractional power, and adsorption isotherm models of Freundlich and Temkin. They suggested that the CFN was taken place on GBC via the mixed mechanism by both physisorption and chemisorption via π–π interactions, hydrogen bonding, n–π interactions, electro donor-acceptor attractions, and electrostatic interaction. Among three studied GBC, GBC700 can be potential adsorbent in the removal of CFN from the aqueous solution. However, the limitation of present study is, the removal of CFN was investigated from a single compound system. Therefore, future investigations to be carried out in the adsorptive removal of CFN from a multi compounds system as well as municipal wastewater under the realistic environmental conditions such as environmental pH and CFN concentration, and the regeneration studies of spend GBC to be investigated in future in order to fulfill the commercial needs.

Declaration of competing interest

The authors declare that they have no known competing financial interests or personal relationships that could have appeared to influence the work reported in this paper.

Acknowledgment

This research was financially supported by a grant (ASP/01/RE/SCI/2018/65) of the Research council, University of Sri Jayewardenepura, Nugegoda, Sri Lanka. Instrument support was provided by the Instrument Centre, and Nanocomposites Research Group at Faculty of Applied Sciences of the University of Sri Jayewardenepura set up by the Accelerating Higher Education Expansion and Development (AHEAD) Operation of the Ministry of Higher Education funded by the World Bank. Further support was received by the Ministry of Education, Youth and Sports of the Czech Republic (CZ.02.1.01/0.0/0.0/16_026/0008403).

References

Ahmad, M., Lee, S.S., Dou, X., Mohan, D., Sung, J.K., Yang, J.E., Ok, Y.S., 2012. Effects of pyrolysis temperature on soybean stover- and peanut shell-derived biochar properties and TCE adsorption in water. Bioresour. Technol. 118, 536–544. https://doi.org/10.1016/j.biortech.2012.05.042.

Ahmad, M., Lee, S.S., Rajapaksha, A.U., Vithanage, M., Zhang, M., Cho, J.S., Lee, S.E., Ok, Y.S., 2013. Trichloroethylene adsorption by pine needle biochars produced at various pyrolysis temperatures. Bioresour. Technol. 143, 615–622. https://doi.org/10.1016/j.biortech.2013.06.033.

Ahmad, M., Rajapaksha, A.U., Lim, J.E., Zhang, M., Bolan, N., Mohan, D., Vithanage, M., Lee, S.S., Ok, Y.S., 2014. Biochar as a sorbent for contaminant management in soil and water: a review. Chemosphere 99, 19–33. https://doi.org/10.1016/j.chemosphere.2013.10.071.

Álvarez, S., Ribeiro, R.S., Gomes, H.T., Sotelo, J.L., García, J., 2015. Synthesis of carbon xerogels and their application in adsorption studies of caffeine and diclofenac as emerging contaminants. Chem. Eng. Res. Des. 95, 229–238. https://doi.org/10.1016/j.cherd.2014.11.001.

Álvarez-Torrellas, S., Rodríguez, A., Ovejero, G., Gómez, J.M., García, J., 2016. Removal of caffeine from pharmaceutical wastewater by adsorption: influence of NOM, textural and chemical properties of the adsorbent. Environ. Technol. 37, 1618–1630. https://doi.org/10.1080/09593330.2015.1122666.

Anastopoulos, I., Katsouromalli, A., Pashalidis, I., 2020. Oxidized biochar obtained from pine needles as a novel adsorbent to remove caffeine from aqueous solutions. J. Mol. Liq. 304, 112661. https://doi.org/10.1016/j.molliq.2020.112661.

A O, D., 2012. Langmuir, Freundlich, Temkin and Dubinin–Radushkevich isotherms studies of equilibrium sorption of Zn 2+ unto phosphoric acid modified rice husk. IOSR J. Appl. Chem. 3, 38–45. https://doi.org/10.9790/5736-0313845.

Ashiq, A., Sarkar, B., Adassooriya, N., Walpita, J., Rajapaksha, A.U., Ok, Y.S., Vithanage, M., 2019. Sorption process of municipal solid waste biochar-montmorillonite composite for ciprofloxacin removal in aqueous media. Chemosphere 236, 124384. https://doi.org/10.1016/j.chemosphere.2019.124384.

Beltrame, K.K., Cazetta, A.L., de Souza, P.S.C., Spessato, L., Silva, T.L., Almeida, V.C., 2018. Adsorption of caffeine on mesoporous activated carbon fibers prepared from pineapple plant leaves. Ecotoxicol. Environ. Saf. 147, 64–71. https://doi.org/10.1016/j.ecoenv.2017.08.034.

Biel-Maeso, M., Corada-Fernández, C., Lara-Martín, P.A., 2018. Monitoring the occurrence of pharmaceuticals in soils irrigated with reclaimed wastewater. Environ. Pollut. 235, 312–321. https://doi.org/10.1016/j.envpol.2017.12.085.

Biswas, K., Saha, S.K., Ghosh, U.C., 2007. Adsorption of fluoride from aqueous solution by a synthetic iron(III)-aluminum(III) mixed oxide. Ind. Eng. Chem. Res. 46, 5346–5356. https://doi.org/10.1021/ie061401b.

Bordoloi, N., Goswami, R., Kumar, M., Kataki, R., 2017. Biosorption of Co (II) from aqueous solution using algal biochar: kinetics and isotherm studies. Bioresour. Technol. 244, 1465–1469. https://doi.org/10.1016/j.biortech.2017.05.139.

Correa-Navarro, Y.M., Moreno-Piraján, J.C., Giraldo, L., Rodríguez-Estupiñan, P., 2019. Caffeine adsorption by fique bagasse biochar produced at various pyrolysis temperatures. Orient. J. Chem. 35, 538–546. https://doi.org/10.13005/ojc/350205.

Correa-Navarro, Y.M., Giraldo, L., Moreno-Piraján, J.C., 2020. Biochar from fique bagasse for remotion of caffeine and diclofenac from aqueous solution. Molecules 25, 1–17. https://doi.org/10.3390/molecules25081849.

de Souza dos Santos, G.E., Ide, A.H., Duarte, J.L.S., McKay, G., Silva, A.O.S., Meili, L., 2020. Adsorption of anti-inflammatory drug diclofenac by MgAl/layered double hydroxide supported on Syagrus coronata biochar. Powder Technol. 364, 229–240. https://doi.org/10.1016/j.powtec.2020.01.083.

Dhir, B., 2019. Removal of Pharmaceuticals and Personal Care Products by Aquatic Plants, Pharmaceuticals and Personal Care Products: Waste Management and Treatment Technology. Elsevier Inc. https://doi.org/10.1016/b978-0-12-816189-0.00014-7.

dos Santos Lins, P.V., Henrique, D.C., Ide, A.H., de Paiva e Silva Zanta, C.L., Meili, L., 2019. Evaluation of caffeine adsorption by MgAl-LDH/biochar composite. Environ. Sci. Pollut. Res. 26, 31804–31811. https://doi.org/10.1007/s11356-019-06288-3.

Ebele, A.J., Abou-Elwafa Abdallah, M., Harrad, S., 2017. Pharmaceuticals and personal care products (PPCPs) in the freshwater aquatic environment. Emerg. Contam. 3, 1–16. https://doi.org/10.1016/j.emcon.2016.12.004.

Emily Chelangat Ngeno, Orata, Francis, Baraza, Lilechi Danstone, Shikuku, Victor Odhiambo, Jemutai Kimosop, Selly, 2016. Adsorption of caffeine and ciprofloxacin onto pyrolitically derived water hyacinth biochar: isothermal, kinetic and thermodynamic studies. J. Chem. Chem. Eng. 10 https://doi.org/10.17265/1934-7375/2016.04.006.

Essandoh, M., Kunwar, B., Pittman, C.U., Mohan, D., Mlsna, T., 2015. Sorptive removal of salicylic acid and ibuprofen from aqueous solutions using pine wood fast pyrolysis biochar. Chem. Eng. J. 265, 219–227. https://doi.org/10.1016/j.cej.2014.12.006.

Guizani, C., Haddad, K., Limousy, L., Jeguirim, M., 2017a. New insights on the structural evolution of biomass char upon pyrolysis as revealed by the Raman spectroscopy and elemental analysis. Carbon N. Y. 119, 519–521. https://doi.org/10.1016/j.carbon.2017.04.078.

Guizani, C., Jeguirim, M., Valin, S., Limousy, L., Salvador, S., 2017b. Biomass chars: the effects of pyrolysis conditions on their morphology, structure, chemical properties and reactivity. Energies 10. https://doi.org/10.3390/en10060796.

Guizani, C., Jeguirim, M., Valin, S., Peyrot, M., Salvador, S., 2019. The Heat Treatment Severity Index: a new metric correlated to the properties of biochars obtained from entrained flow pyrolysis of biomass. Fuel 244, 61–68. https://doi.org/10.1016/j.fuel.2019.01.170.

Herman, A., Herman, A.P., 2012. Caffeine's mechanisms of action and its cosmetic use. Skin Pharmacol. Physiol. 26, 8–14. https://doi.org/10.1159/000343174.

Inyinbor, A.A., Adekola, F.A., Olatunji, G.A., 2016. Kinetics, isotherms and thermodynamic modeling of liquid phase adsorption of Rhodamine B dye onto Raphia hookerie fruit epicarp. Water Resour. Ind. 15, 14–27. https://doi.org/10.1016/j.wri.2016.06.001.

Jiang, J., Zhang, L., Wang, X., Holm, N., Rajagopalan, K., Chen, F., Ma, S., 2013. Highly ordered macroporous woody biochar with ultra-high carbon content as supercapacitor electrodes. Electrochim. Acta 113, 481–489. https://doi.org/10.1016/j.electacta.2013.09.121.

Jiang, X., Ouyang, Z., Zhang, Z., Yang, C., Li, X., Dang, Z., Wu, P., 2018. Mechanism of glyphosate removal by biochar supported nano-zero-valent iron in aqueous solutions. Colloids Surfaces A Physicochem. Eng. Asp. 547, 64–72. https://doi.org/10.1016/j.colsurfa.2018.03.041.

Kawakami, M., Karato, T., Takenaka, T., Yokoyama, S., 2005. Structure analysis of coke, wood charcoal and bamboo charcoal by Raman spectroscopy and their reaction rate with CO2. ISIJ Int. 45, 1027–1034. https://doi.org/10.2355/isijinternational.45.1027.

Keerthanan, S., Bhatnagar, A., Mahatantila, K., Jayasinghe, C., Ok, Y.S., Vithanage, M., 2020a. Engineered tea-waste biochar for the removal of caffeine, a model compound in pharmaceuticals and personal care products (PPCPs), from aqueous media. Environ. Technol. Innov. 19, 100847. https://doi.org/10.1016/j.eti.2020.100847.

Keerthanan, S., Jayasinghe, C., Biswas, J.K., Vithanage, M., 2020b. Pharmaceutical and Personal Care Products (PPCPs) in the environment: plant uptake, translocation, bioaccumulation, and human health risks. Crit. Rev. Environ. Sci. Technol. 1–38. https://doi.org/10.1080/10643389.2020.1753634.

Kleywegt, S., Payne, M., Raby, M., Filippi, D., Ng, C.F., Fletcher, T., 2019. The final discharge: quantifying contaminants in embalming process effluents discharged to sewers in ontario, Canada. Environ. Pollut. 252, 1476–1482. https://doi.org/10.1016/j.envpol.2019.06.036.

Kong, S.H., Lam, S.S., Yek, P.N.Y., Liew, R.K., Ma, N.L., Osman, M.S., Wong, C.C., 2019. Self-purging microwave pyrolysis: an innovative approach to convert oil palm shell into carbon-rich biochar for methylene blue adsorption. J. Chem. Technol. Biotechnol. 94, 1397–1405. https://doi.org/10.1002/jctb.5884.

Kumar, M., Ram, B., Honda, R., Poopipattana, C., Canh, V.D., Chaminda, T., Furumai, H., 2019. Concurrence of antibiotic resistant bacteria (ARB), viruses, pharmaceuticals and personal care products (PPCPs) in ambient waters of Guwahati, India: urban vulnerability and resilience perspective. Sci. Total Environ. 693, 133640. https://doi.org/10.1016/j.scitotenv.2019.133640.

Lee, H.J., Kim, K.Y., Hamm, S.Y., Kim, M.S., Kim, H.K., Oh, J.E., 2019. Occurrence and distribution of pharmaceutical and personal care products, artificial sweeteners, and pesticides in groundwater from an agricultural area in Korea. Sci. Total Environ. 659, 168–176. https://doi.org/10.1016/j.scitotenv.2018.12.258.

Li, J., Yu, G., Pan, L., Li, C., You, F., Xie, S., Wang, Y., Ma, J., Shang, X., 2018. Study of ciprofloxacin removal by biochar obtained from used tea leaves. J. Environ. Sci. (China) 73, 20–30. https://doi.org/10.1016/j.jes.2017.12.024.

Li, S., Wen, J., He, B., Wang, J., Hu, X., Liu, J., 2020a. Occurrence of caffeine in the freshwater environment: implications for ecopharmacovigilance. Environ. Pollut. 263, 114371. https://doi.org/10.1016/j.envpol.2020.114371.

Li, X., Wang, C., Tian, J., Liu, J., Chen, G., 2020b. Comparison of adsorption properties for cadmium removal from aqueous solution by Enteromorpha prolifera biochar modified with different chemical reagents. Environ. Res. 186, 109502. https://doi.org/10.1016/j.envres.2020.109502.

Lin, T., Yu, S., Chen, W., 2016. Occurrence, removal and risk assessment of pharmaceutical and personal care products (PPCPs) in an advanced drinking water treatment plant (ADWTP) around Taihu Lake in China. Chemosphere 152, 1–9. https://doi.org/10.1016/j.chemosphere.2016.02.109.

Liu, J.L., Wong, M.H., 2013. Pharmaceuticals and personal care products (PPCPs): a review on environmental contamination in China. Environ. Int. 59, 208–224. https://doi.org/10.1016/j.envint.2013.06.012.

Liu, X.F., You, J.L., Wang, Y.Y., Lu, L.M., Xie, Y.F., Yu, L.W., Fu, Q., 2014. Raman spectroscopic study on the pyrolysis of Australian bituminous coal. Ranliao Huaxue Xuebao/J. Fuel Chem. Technol. 42, 270–276. https://doi.org/10.1016/s1872-5813(14)60019-0.

Madikizela, L.M., Ncube, S., Chimuka, L., 2018. Uptake of pharmaceuticals by plants grown under hydroponic conditions and natural occurring plant species: a review. Sci. Total Environ. 636, 477–486. https://doi.org/10.1016/j.scitotenv.2018.04.297.

Maliutina, K., Tahmasebi, A., Yu, J., 2018. Effects of pressure on morphology and structure of bio-char from pressurized entrained-flow pyrolysis of microalgae. Data Br 18, 422–431. https://doi.org/10.1016/j.dib.2018.03.048.

Mayakaduwa, S.S., Kumarathilaka, P., Herath, I., Ahmad, M., Al-Wabel, M., Ok, Y.S., Usman, A., Abduljabbar, A., Vithanage, M., 2016a. Equilibrium and kinetic

mechanisms of woody biochar on aqueous glyphosate removal. Chemosphere 144, 2516–2521. https://doi.org/10.1016/j.chemosphere.2015.07.080.
Mayakaduwa, S.S., Vithanage, M., Karunarathna, A., Mohan, D., Ok, Y.S., 2016b. Interface interactions between insecticide carbofuran and tea waste biochars produced at different pyrolysis temperatures. Chem. Speciat. Bioavailab. 28, 110–118. https://doi.org/10.1080/09542299.2016.1198928.
McDonald-Wharry, J., Manley-Harris, M., Pickering, K., 2013. Carbonisation of biomass-derived chars and the thermal reduction of a graphene oxide sample studied using Raman spectroscopy. Carbon N. Y. 59, 383–405. https://doi.org/10.1016/j.carbon.2013.03.033.
Mendonça, F.G. de, Cunha, I.T. da, Soares, R.R., Tristão, J.C., Lago, R.M., 2017. Tuning the surface properties of biochar by thermal treatment. Bioresour. Technol. 246, 28–33. https://doi.org/10.1016/j.biortech.2017.07.099.
Ncibi, M.C., Ranguin, R., Pintor, M.J., Jeanne-Rose, V., Sillanpää, M., Gaspard, S., 2014. Preparation and characterization of chemically activated carbons derived from Mediterranean Posidonia oceanica (L.) fibres. J. Anal. Appl. Pyrolysis 109, 205–214. https://doi.org/10.1016/j.jaap.2014.06.010.
Netzahuatl-Muñoz, A.R., Del Carmen Cristiani-Urbina, M., Cristiani-Urbina, E., 2015. Chromium biosorption from Cr(VI) aqueous solutions by Cupressus lusitanica bark: kinetics, equilibrium and thermodynamic studies. PloS One 10, 1–23. https://doi.org/10.1371/journal.pone.0137086.
Panthi, S., Sapkota, A.R., Raspanti, G., Allard, S.M., Bui, A., Craddock, H.A., Murray, R., Zhu, L., East, C., Handy, E., Callahan, M.T., Haymaker, J., Kulkarni, P., Anderson, B., Craighead, S., Gartley, S., Vanore, A., Betancourt, W.Q., Duncan, R., Foust, D., Sharma, M., Micallef, S.A., Gerba, C., Parveen, S., Hashem, F., May, E., Kniel, K., Pop, M., Ravishankar, S., Sapkota, A., 2019. Pharmaceuticals, herbicides, and disinfectants in agricultural water sources. Environ. Res. 174, 1–8. https://doi.org/10.1016/j.envres.2019.04.011.
Papageorgiou, M., Zioris, I., Danis, T., Bikiaris, D., Lambropoulou, D., 2019. Comprehensive investigation of a wide range of pharmaceuticals and personal care products in urban and hospital wastewaters in Greece. Sci. Total Environ. 694, 133565. https://doi.org/10.1016/j.scitotenv.2019.07.371.
Pavia, Donald L., Gary, M., Lampman, G.S.K., 2001. Pavia - Introduction to Spectroscopy - Guide for Students of Organic Chemistry 3e (Thomson, 2001).pdf, Third. ed. Thomson Learning, Inc., USA.
Ptaszkowska-Koniarz, M., Goscianska, J., Pietrzak, R., 2018. Synthesis of carbon xerogels modified with amine groups and copper for efficient adsorption of caffeine. Chem. Eng. J. 345, 13–21. https://doi.org/10.1016/j.cej.2018.03.132.
Rajapaksha, A.U., Vithanage, M., Zhang, M., Ahmad, M., Mohan, D., Chang, S.X., Ok, Y. S., 2014. Pyrolysis condition affected sulfamethazine sorption by tea waste biochars. Bioresour. Technol. 166, 303–308. https://doi.org/10.1016/j.biortech.2014.05.029.
Rajapaksha, A.U., Vithanage, M., Ahmad, M., Seo, D.C., Cho, J.S., Lee, S.E., Lee, S.S., Ok, Y.S., 2015. Enhanced sulfamethazine removal by steam-activated invasive plant-derived biochar. J. Hazard Mater. 290, 43–50. https://doi.org/10.1016/j.jhazmat.2015.02.046.
Shen, Q., Wang, Z., Yu, Q., Cheng, Y., Liu, Z., Zhang, T., Zhou, S., 2020. Removal of tetracycline from an aqueous solution using manganese dioxide modified biochar derived from Chinese herbal medicine residues. Environ. Res. 183, 109195. https://doi.org/10.1016/j.envres.2020.109195.
Su, M.H., Azwar, E., Yang, Y.F., Sonne, C., Yek, P.N.Y., Liew, R.K., Cheng, C.K., Show, P. L., Lam, S.S., 2020. Simultaneous removal of toxic ammonia and lettuce cultivation in aquaponic system using microwave pyrolysis biochar. J. Hazard Mater. 396, 122610. https://doi.org/10.1016/j.jhazmat.2020.122610.
Tomczyk, A., Sokołowska, Z., Boguta, P., 2020. Biochar physicochemical properties: pyrolysis temperature and feedstock kind effects. Rev. Environ. Sci. Biotechnol. 19, 191–215. https://doi.org/10.1007/s11157-020-09523-3.
Tran, H.N., Wang, Y.F., You, S.J., Chao, H.P., 2017a. Insights into the mechanism of cationic dye adsorption on activated charcoal: the importance of Π–Π interactions. Process Saf. Environ. Protect. 107, 168–180. https://doi.org/10.1016/j.psep.2017.02.010.
Tran, H.N., You, S.J., Chao, H.P., 2017b. Fast and efficient adsorption of methylene green 5 on activated carbon prepared from new chemical activation method. J. Environ. Manag. 188, 322–336. https://doi.org/10.1016/j.jenvman.2016.12.003.
Tran, H.N., You, S.J., Hosseini-Bandegharaei, A., Chao, H.P., 2017c. Mistakes and inconsistencies regarding adsorption of contaminants from aqueous solutions: a critical review. Water Res. 120, 88–116. https://doi.org/10.1016/j.watres.2017.04.014.
Vithanage, M., Mayakaduwa, S.S., Herath, I., Ok, Y.S., Mohan, D., 2016. Kinetics, thermodynamics and mechanistic studies of carbofuran removal using biochars from tea waste and rice husks. Chemosphere 150, 781–789. https://doi.org/10.1016/j.chemosphere.2015.11.002.
Wang, J., Wang, S., 2016. Removal of pharmaceuticals and personal care products (PPCPs) from wastewater: a review. J. Environ. Manag. 182, 620–640. https://doi.org/10.1016/j.jenvman.2016.07.049.
Yadav, L.D.S., 2002. Organic spectroscopy. J. Chem. Edu. Springer Sci. Bus. Media. https://doi.org/10.1042/bst0040394.
Yanala, S.R., Pagilla, K.R., 2020. Use of biochar to produce reclaimed water for irrigation use. Chemosphere 251, 126403. https://doi.org/10.1016/j.chemosphere.2020.126403.
Yang, X., Kwon, E.E., Dou, X., Zhang, M., Kim, K.H., Tsang, D.C.W., Ok, Y.S., 2018. Fabrication of spherical biochar by a two-step thermal process from waste potato peel. Sci. Total Environ. 626, 478–485. https://doi.org/10.1016/j.scitotenv.2018.01.052.
Yip, K., Xu, M., Li, C.Z., Jiang, S.P., Wu, H., 2011. Biochar as a fuel: 3. Mechanistic understanding on biochar thermal annealing at mild temperatures and its effect on biochar reactivity. Energy Fuel. 25, 406–414. https://doi.org/10.1021/ef101472f.
Zhang, Y.J., Xing, Z.J., Duan, Z.K., Li, M., Wang, Y., 2014. Effects of steam activation on the pore structure and surface chemistry of activated carbon derived from bamboo waste. Appl. Surf. Sci. 315, 279–286. https://doi.org/10.1016/j.apsusc.2014.07.126.
Zhang, X., Zhang, P., Yuan, X., Li, Y., Han, L., 2020. Effect of pyrolysis temperature and correlation analysis on the yield and physicochemical properties of crop residue biochar. Bioresour. Technol. 296, 122318. https://doi.org/10.1016/j.biortech.2019.122318.
Zhao, B., O'Connor, D., Zhang, J., Peng, T., Shen, Z., Tsang, D.C.W., Hou, D., 2018. Effect of pyrolysis temperature, heating rate, and residence time on rapeseed stem derived biochar. J. Clean. Prod. 174, 977–987. https://doi.org/10.1016/j.jclepro.2017.11.013.